An update on the wind power input to the surface geostrophic flow of the World Ocean

Robert B. Scott [a,*]

[a] *Institute for Geophysics, Jackson School of Geosciences University of Texas at Austin JJ Pickle Research Campus, Bldg. 196 (ROC) 10100 Burnet Rd. (R2200), Austin, TX 78759, U.S.A*

Yongsheng Xu [a,b]

[b] *Department of Geological Sciences, Jackson School of Geosciences University of Texas at Austin, 23rd Street at San Jacinto Blvd., Austin, TX 78705, U.S.A*

Abstract

The rate of working of the surface wind stress on the geostrophic component of the surface flow of the World Ocean is revisited. The global mean is found to be about 0.85 to 1.0 TW. Consistent with previous estimates, about 0.75 to 0.9 TW comes from outside the equatorial region. The rate of forcing of fluctuating currents is only about 0.02 TW, almost all of which is found within 3° of the equator. Uncertainty in wind power input due to uncertainty in the wind stress and surface currents is addressed. Results from several different wind stress products are compared, suggesting that uncertainty in wind stress is the dominant source of error. Ignoring the surface currents' influence upon wind stress leads to a systematic bias in net wind power input; an overestimate of about 10 to 30%. (In previous estimates this positive bias was offset by too weak winds.) Small-scale, zonally elongated structures in the wind power input were found, but have both positive and negative contributions and lead to little net wind power input.

Key words:
Ocean energetics, Wind stress, World Ocean, Diapycnal mixing
PACS: 92.10.ab, 92.10.Kp

---

1 Introduction

1.1 The mechanical energy budget and diapycnal mixing

Understanding the mechanical energy budget of the World Ocean is important and interesting for several reasons. Anticipating the intensity and distribution of this diapycnal mixing requires knowledge of the sources of mechanical energy and pathways and processes that lead to mechanical energy dissipation (Munk and Wunsch, 1998; Wunsch and Ferrari, 2004).

Surface stress working on the ocean surface and tides represent the major mechanical energy inputs. Huang et al. (2006) make the interesting point that while tidal dissipation is important for understanding the present MOC, and possibly paleoclimate (e.g. Arbic et al., 2004), it probably plays little role in climate variability on subcentennial timescales. In contrast, the wind power from surface stress working on the surface flow can fluctuate considerably from year to year.

* Corresponding author. Tel.: +1 512 471-0375; fax: +1 512 471-8844
Email address: `rscott@ig.utexas.edu` (Robert B. Scott).

The other surface stress power sources are probably of less interest to abyssal mixing. The normal stress working on vertical displacements of the surface leads to only about 0.01 TW, at least for non-tidal frequencies (Wunsch and Ferrari, 2004). While substantial power goes into the surface Ekman currents, about 2.4 TW (Wang and Huang, 2004a), much of this will be dissipated within the Ekman layer (upper few tens of meters) and therefore not available to drive diapycnal mixing deeper in the water column. Enormous power is transferred to the surface waves – about 60 TW; however it's not clear how much of this is transfer below the surface mixed layer (Wang and Huang, 2004b).

Two pathways of mechanical energy from the surface to the deeper ocean are clear at present: wind forcing of near inertial oscillations and wind forcing of surface geostrophic flow. Estimates of the former are between 0.5 to 0.7 TW of power (Alford, 2003; Watanabe and Hibiya, 2002), but these may be overestimates (Plueddemann and Farrar, 2006). The latter is the focus of the current study. A more accurate estimate of this power source, and an estimate of the range of uncertainty, will help constrain our currently fuzzy picture of the processes driving diapycnal mixing.

1.2 Previous estimates of wind power to surface geostrophic flow

Several observational estimates of the wind power to the surface geostrophic flow have been made. Prior to the satellite era, only rough estimates were possible(e.g. Oort et al., 1994). Using the TOPEX/Poseidon altimeter data relative to EGM-96 geoid and NCEP wind stress, Wunsch (1998) estimated 0.9 TW of wind power, excluding the region within 3 degrees of the Equator and beyond the region covered by the satellite data (poleward of about 63°), though Wunsch emphasized the "potentially large uncertainty". Independently, the first author made a very similar calculation for his Ph.D. research, and estimated the errors from the JGM-3 error covariance matrix to be around 6%(Scott, 1999a). The error estimate methodology was also explained by Scott (1999b). This suggests that little is to be gained by improving estimates of the mean flow at least at large scales, but the question of the role of small scales not resolved by the single-satellite altimeter data and the JGM-3 geoid (to degree and order 70) remains.

Several estimates have been made using ocean models, all giving similar results (Wunsch, 1998; Huang et al., 2006; von Storch et al., 2007). Note that *all* these model-based results used NCEP wind stress. Large errors arising from the surface wind stress remains a troubling possibility since systematic biases in the reanalysis stress are conceivable. The present work attempts to quantify this uncertainty.

1.3 Goals of this work

Here we calculate the wind power input to the geostrophic flow $\dot{W}_g$ using near global satellite data of surface currents and wind stress. We're especially interested in the time mean, global integral, which hereinafter we refer to as "wind power input", WPI (keeping in mind that the winds do force other motions, such as inertial oscillations, which must be considered separately). Our goal is to constrain the uncertainty, which, with the exception of the influence of geoid gradient errors (Scott, 1999a), was not quantified in previous estimates of WPI. In section 2 we argue for the simple formulation of the $\dot{W}_g$, and emphasize the subtle influence of the surface currents on wind stress. The data sets used in this study, and the preprocessing are discussed in section 3. Results are presented in section 4, and implications discussed in section 5.

2 Background

The rate of working on the ocean at the air-sea interface is derived from Newton's laws of motion,

$$\dot{W} = \vec{u}_s \cdot \vec{\tau} \tag{1}$$

where $\vec{u}_s$ is the three dimensional surface current and $\vec{\tau}$ is the surface stress including the pressure normal to the surface. The surface current is in general composed of many components, and can be decomposed in several ways. Here we're only interested in the horizontal geostrophic flow, and so we decompose $\vec{u}_s$ into geostrophic and ageostrophic components,

$$\vec{u}_s = \vec{u}_g + \vec{u}_a. \tag{2}$$

Substituting the decomposition of Equation 2 into Equation 1 we find the rate of working on the geostrophic flow is simply

$$\dot{W}_g = \vec{u}_g \cdot \vec{\tau}_s, \tag{3}$$

where $\vec{\tau}_s$ is the (horizontal) shear stress.

Through much more detailed consideration of the atmospheric and oceanic boundary layers, Bye arrives at an equivalent expression (Bye, 1985, Equation

10), for the flux of mechanical energy to the currents below the oceanic boundary layer near the air-sea interface, denoted $\vec{u}_o$ in his notation. Bye notes that $\vec{u}_o \approx \vec{u}_g$. Previous estimates of the wind power input to the oceanic general circulation(e.g. Wunsch, 1998; Oort et al., 1994) also use Equation 3, assuming that wind power to ageostrophic motions do not feed into the general circulation. Supporting this assumption, von Storch et al. (2007) found very close agreement between the wind power to the surface geostrophic flow (1.06 TW) and the flux of mechanical energy to the deeper ocean across the 110 m depth surface (1.1 TW). Note that near inertial oscillations are not resolved by the daily sampling used in the von Storch et al. study.

The surface shear stress, $\vec{\tau}_s$, is typically parameterized as

$$\vec{\tau}_s = \rho_a \, c_d \, |\vec{U}_a - \vec{u}_s|(\vec{U}_a - \vec{u}_s), \tag{4}$$

where $\rho_a \approx 1.2$ kg m^{-3} is the air density, $\vec{U}_a$ is the surface wind velocity at some reference height (typically 10 m above sea level), and $c_d = O(10^{-3})$ is the dimensionless drag coefficient. c_d itself is a weak function of the surface wind speed and stability of the boundary layer; see Brunke et al. (2003) for a comprehensive comparison of algorithms.

Typically $|\vec{u}_s| \ll |\vec{U}_a|$, and so $\vec{\tau}_s$ is not affected much by the surface current. However, $\vec{u}_s$ and $\vec{U}_a$ are also not well correlated, and so a somewhat subtle implication of Equation 3 is that $\dot{W}_g$ can be strongly effected by the surface flow (Bye, 1985; Duhaut and Straub, 2006; Dawe and Thompson, 2006). The current authors have quantified this effect for the real ocean, suggesting that it leads to about a reduction in $\dot{W}_g$ of about one third, and much more in very energetic areas. We also argue that it might lead to about one quarter too much wind power input to an ocean only general circulation model forced with observed wind stress (Xu and Scott, 2008). Hughes and Wilson (2008) have also quantified this effect for the real ocean using a complementary approach.

3 Data

3.1 Recent improvements to global wind and current data sets

Improvements in data allow us to make a better estimate than ten years ago, and allow us to assess the error. Rigorous error estimates are generally not feasible when combining several global geophysical data sets, even when error bars are available for the individual products. (Here we would need the joint error covariance matrix for both wind stress and surface currents.) In lieu of this, we consider the range of results obtained with different data sets. All the data sets used are described in more detail in section 3. The most significant improvement is the availability of multi-year, near global wind stress fields from satellite based scatterometers(Kelly, 2004). Sea-surface height anomaly fields combining altimeter data from multiple satellites has greatly improved our ability to resolve mesoscale eddies(Pascual et al., 2007). The geoid is greatly improved by the GRACE mission, and the mean sea surface (MSS) has much higher resolution through combining data from many satellites with different ground tracks. Finally, methodologies that combine hydrographic and surface drifter data with the MSS from altimetry relative to the geoid allow for improved estimates of the mean circulation(Rio and Hernandez, 2004; Niiler et al., 2003).

3.2 Surface geostrophic currents

Higher spatial resolution and accurate surface currents are now possible because between two and four satellites are simultaneously monitoring the ocean. We use AVISO merged data of absolute geostrophic velocity compiled by the CLS Space Oceanographic Division of Toulouse, France. These data are provided as weekly averages on a 1/3° longitude Mercator grid, though temporal and spatial smoothing result in slightly less resolution(LeTraon et al., 1998; Ducet et al., 2000; LeTraon et al., 2001). Both a "reference" and an"updated" product are available. The "reference" product merges at most two satellites (one with 10-day repeat orbit (either Topex/Poseidon or Jason-1) and the other with 35-day repeat orbit (either ERS1 or ERS2 or Envisat)). This product sacrifices resolution and accuracy for data quality homogeneity in time. The "updated" product merges up to four satellites (Topex/Poseidon and Jason-1, ERS1/2, Envisat, Geosat follow-on) at a given time and has a much improved capability of detecting the mesoscale signals than a single satellite(Pascual et al., 2007).

3.2.1 Mean currents

The AVISO altimeter products use the Rio05 mean dynamic topography (MDT), described at http://www.jason.oceanobs.com/html/donnees/produits /auxiliaires/rio05_uk.html. Note that this product uses the GRACE mission geoid(Tapley et al., 2003; Reigber et al., 2005) for wavelengths larger than 400km, where the errors are much smaller than the EGM96 geoid used in the previous $\dot{W}_g$ estimates. They also combine *in situ* hydrographic and surface drifter data to obtain better estimates of the time mean surface currents at length scales not well resolved by GRACE; the methodology is described by Rio and Hernandez (2004), as applied to an earlier gravity model. The fields are smoothed over 1° longitude by 1/2° latitude.

For comparison, we also used the AVISO surface current anomalies (relative to the 7-year mean from 1993 through 1999) in combination with the Maximenko MDT(Niiler et al., 2003), and with the GRACE-Tellus MDT(Tapley et al., 2003). The Maximenko MDT applies a similar methodology as the Rio05 MDT, in this case blending the GRACE-Tellus MDT at the large scales with surface drifter information at smaller scales. The Ekman component of the current is removed from the drifter velocity at 6-hr intervals using an empirical relation between 10 m winds and Ekman current at 15 m depth (Ralph and Niiler, 1999). The winds were taken from the NCEP reanalysis (Niiler et al., 2003). The GRACE-Tellus MDT used the mean sea surface from altimetry relative to the geoid from 363 days of the GRACE mission (GGM02C), both filtered to about 400 km wavelength. [1]

3.3 Surface wind stress

We compare the wind power input results obtained with several wind stress products. Our best estimate comes from scatterometer data of NASA's QuikSCAT satellite, described in more detail below. This product naturally takes account of the surface currents influence on stress. For comparison we also use

[1] The filtering process and all preprocessing steps are clearly described in the power point presentation by Don Chambers, available on the JPL website http://gracetellus.jpl.nasa.gov/dot.html. Note however, that the summary on the website is not correct (Don Chambers, personal communication).

wind stress from reanalysis of meteorological data, the NCEP2 reanalysis and ECMWF's ERA-40. These products have much lower spatial resolution and are based only upon the surface winds, ignoring $\vec{u}_s$ in Equation 4 above.

To roughly account for the surface current effect on stress in the reanalysis wind products, we used their daily averaged 10 m height wind speeds, $\vec{U}_a$, and wind stresses $\vec{\tau}_R$, to infer the air density and drag coefficient used by the model,

$$\rho_a \; c_d = \frac{|\vec{U}_a|^2}{|\vec{\tau}_R|}.$$

We then used the AVISO surface geostrophic currents, smoothed with a 2° longitude Gaussian filter to approximate the resolution of the reanalysis winds and interpolated to daily values, to approximate the $\vec{u}_s$ in Equation 4. This provided a low-resolution stress that approximately accounts for the surface currents. Because the energy containing scales of the ocean are between 300 km to 400 km wavelength (Stammer, 1997; Scott and Wang, 2005), unfortunately much of the negative wind power input resulting from the surface current effect on stress cannot be resolved by the reanalysis wind products. Note that the true surface current includes non-geostrophic components. But this likely leads to very small error for the computation of $\dot{W}_g$ because of the projection upon $\vec{u}_g$.

3.3.1 QuikSCAT

The SeaWinds scatterometer on the QuikSCAT satellite measures the near surface wind vectors from the radar backscatter signal associated with small surface waves generated by the surface stress at the air-sea interface. Thus the scatterometer derived wind stress naturally accounts for the surface current effect on stress, as well the static stability of the atmosphere which can decrease the drag coefficient c_d. QuikSCAT samples about 90% of the ice-free World Ocean every 24 hours with a grid resolution of 25 km, more than an order of magnitude better than reanalysis wind stress (Kelly, 2004). The accuracy of the vector winds is comparable to that of *in situ* point measurements from buoys(Chelton and Freilich, 2005). The daily QuikSCAT level 3-derived global 0.25° neutral vector wind data is used in this study, JPL PO.DAAC product 109(Perry, 2001). We converted the 10 m winds of both the ascending and descending passes into stresses using the Liu and Tang or the Large and Pond algorithm (both of which are described by Brunke et al. (2003)). These stresses were averaged to form daily averaged stress.

3.3.2 Other wind products

GSSFT2 is a daily global 1° × 1° resolution surface stress product derived from satellite SSM/I wind speed estimates and wind directions from *in situ* and NCEP/NCAR reanalysis winds(Chou et al., 2004). Because the wind direction involves reanalysis data GSSFT2 imperfectly accounts for the surface current reduction in surface stress.

NCEP2(Kanamitsu et al., 2000) is an update on the NCEP/NCAR reanalysis(Kistler et al., 2001). It improves upon the known problems of too weak winds in the tropics in the NCEP/NCAR reanalysis(Wittenberg, 2004). The spatial resolution is 1.875° longitude by roughly 1.9° latitude. We use the daily mean stress and 10 m winds to infer the stress with and without the surface current effect included.

ERA-40 is the forty year ECMWF reanalysis. We used the $2.5° \times 2.5°$ resolution, four times daily stress and 10 m winds to infer the daily stress with and without the ocean surface current effect.

It is important to keep in mind that the surface current effect was seriously limited by the spatial resolution of both reanalysis wind products (NCEP2 and ERA-40).

4 Results

WPI, the time mean, global integrals of $\dot{W}_g$, using the various data products are summarized in Table 1. The first row shows our best estimate, using QuikSCAT wind stress and the updated AVISO geostrophic currents, see also Fig. 1. To facilitate comparison between products, that in general have different missing data points, we replaced missing data points with values from our best estimate. Furthermore, all integrals are carried out only over the area used for this best estimate (hereafter the 'reference area', which is the area in Fig. 1); the column labelled 'area' in Table 1 shows the fraction of this area for which data was available. We excluded grid points for which less than 52 weeks of good data were available. This removed the grid points near the ice edge, especially near the southern boundary, where the data are suspect; however, this had a negligible influence on WPI. Both global and extraequatorial results are presented in Table 1, the latter excluding the region within 3° degrees of the equator. The extraequatorial results were added, at the request of an anonymous reviewer, to facilitate comparison with previous estimates, and because the equatorial currents are more suspect.

Our best estimate for the global integral of $\dot{W}_g = 0.91$ TW is fortuitously close to that obtained previously using NCEP wind stress and TOPEX/Poseidon currents: 0.88 TW by Wunsch (1998), 0.77 TW by Scott (1999b), and 0.84 TW by Huang et al. (2006). However, those earlier estimates excluded the region between 3° S and 3° N, which is a region of strong positive wind power input, see Fig. 1, (and note Wunsch and Scott excluded depths less than 1000 m and 500 m respectively). If we exclude the region 3° S and 3° N, we find 0.81 TW. Excluding both the equatorial region and depths less than 1000 m (2000 m) reduces the WPI to 0.78 TW (0.77 TW). The spatial distribution of the power input has been discussed in other recent studies(Xu and Scott, 2008; Hughes and Wilson, 2008), so here we focus on the uncertainty. For completeness, Fig. 1 shows the map of our best estimate of $\dot{W}_g$ using QuikSCAT wind stress and the updated AVISO geostrophic currents.

4.1 Uncertainty arising from uncertainty in geostrophic currents

The much higher spatial resolution of both surface geostrophic currents and wind stress in Fig. 1 has revealed alternating, zonally aligned bands of positive and negative $\dot{W}_g$. However, these small-scale features contribute very little to the global WPI. This was determined by recalculating $\dot{W}_g$ using the much smoother GRACE-Tellus MDT, see section 3.2.1, which affectively eliminates $\dot{W}_g$ from scales smaller than about 400 km wavelength, see the map of $\dot{W}_g$ shown in Fig. 2. Yet the WPI changed only by about 0.01 TW.

As a second check on the influence of the small scales, we redid the WPI calculation with mean currents from the Maximenko MDT (see section 3.2) and the geostrophic current anomalies from the updated AVISO currents relative

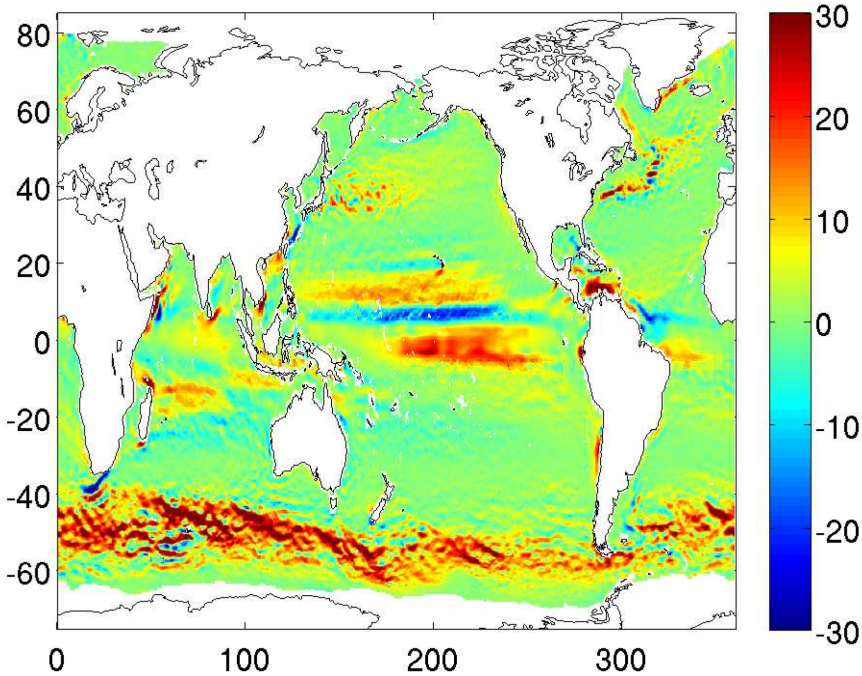

Fig. 1. Our best estimate of $\dot{W}_g$ using data corresponding to row one of Table 1. Units: mWm^{-2}. Color-shaded region also corresponds to the reference area, $3.14 \times 10^{14}\mathrm{m}^2$ in total, over which all other estimates in Table 1 were integrated. Where data were missing for those other estimates, the field shown here was substituted.

to a 7-year mean. Most of the small-scale features corresponded to qualitatively similar, albeit somewhat distorted, features found with the AVISO mean currents. So we believe these are real features, though not quantitatively accurate. Fortunately they contribute little, and therefore don't adversely affect the WPI accuracy. Using the Maximenko MDT instead of the Rio05 MDT of AVISO changed the WPI only by a about 0.01 TW (or 9.6 GW) (compare first and third rows of Table 1), implying that the WPI is not sensitive to the details of the small-scale mean currents.

Because the wind stress anomalies working on the current anomalies (the

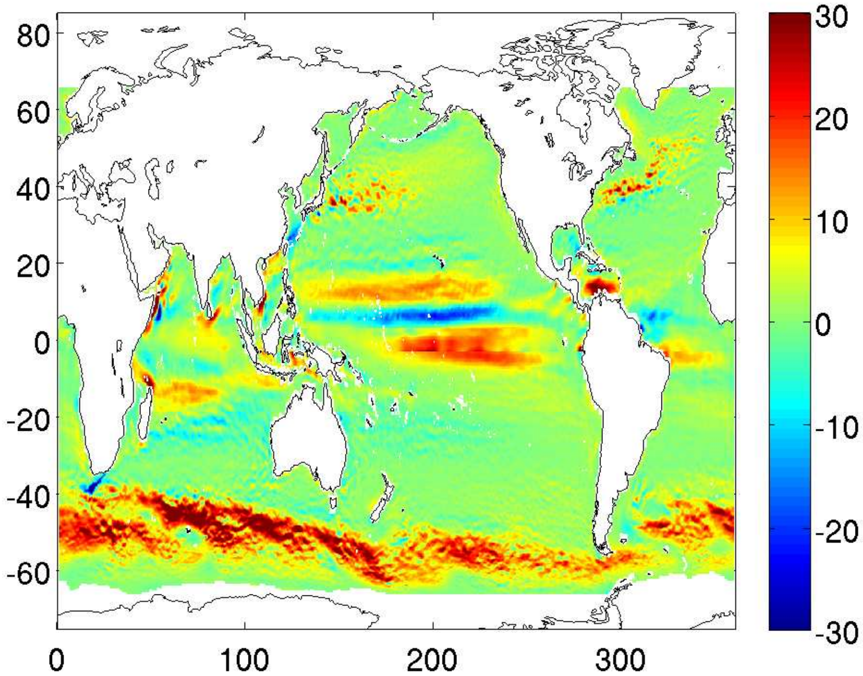

Fig. 2. $\dot{W}_g$ using data corresponding to row two of Table 1. Units: mWm^{-2}. Note that most of the deep blue streaks of Fig. 1 have been eliminated by the much smoother GRACE-Tellus mean dynamic topography.

"Eddy WPI" column) amounts to very little of the total mean power input, sensitivity to the current anomalies is not a major concern. We confirmed this by using the AVISO reference product instead of the updated product, effectively reducing the spatial resolution and quality of the current anomalies. The eddy WPI was affected by only 1 GW, see row four of Table 1. WPI changed a similar amount, from $0.9077 \rightarrow 0.9094$ TW. (This many significant figures are not included in Table 1 in keeping with the confidence in the absolute results.)

Anonymous reviewers pointed out that the updated AVISO product has limited spatial resolution, and raised concern over the unresolved eddy WPI. Hughes and Wilson (2008) found that the small scales have negative WPI, so we suspect that the unresolved Eddy WPI tends to reduce the true Eddy WPI to levels even smaller than the approximate 20 GW resolved here. Is it possible that the true Eddy WPI is negative, perhaps significantly so? The following simple argument suggests that the true Eddy WPI is actually indistinguishable from zero.

Consider a Gaussian eddy under a uniform reference level wind. (Of course this does not address correlations in the spatial pattern of winds and surface geostrophic currents.) Without further loss of generality, we consider the case of an anticyclone in the Northern Hemisphere under a westerly wind. Figure 3 shows the resulting dipole in wind power input. The dipole is not quite antisymmetric about the latitude line through the eddy center; compare for instance the $\pm$ 3mW/m^2 contours shown in bold. In particular, the northern half of the eddy, where the current and wind stress are aligned has smaller positive input, while the southern half of the eddy, where the wind and currents are opposed, has slightly larger negative input. This arises from the surface current effect on the wind stress, see also Xu and Scott (2008, Figure 1). The case shown is meant to represent typical midlatitude conditions: $\rho_a = 1.2$ kg/m^3, $c_d = 0.001$, $f = 1 \times 10^{-4}$ rad/s, with moderate winds $U_a = 5$ m/s. The eddy has Gaussian width 25 km and amplitude of 5 cm, so a fairly strong eddy with currents reaching 12 cm/s. The average wind power input over the area shown is -0.05 mW/m^2. Multiplying this by the reference area of 3.14×10^{14}m^2, we find a global contribution of -15 GW. For quite vigorous winds of $U_a = 10$ m/s, the global contribution is -30 GW. With the best estimate of resolved Eddy WPI of 24 GW, this suggests the true Eddy WPI is indistinguishable from zero.

Figure 4 shows plots of the zonal integral of WPI using data from the first

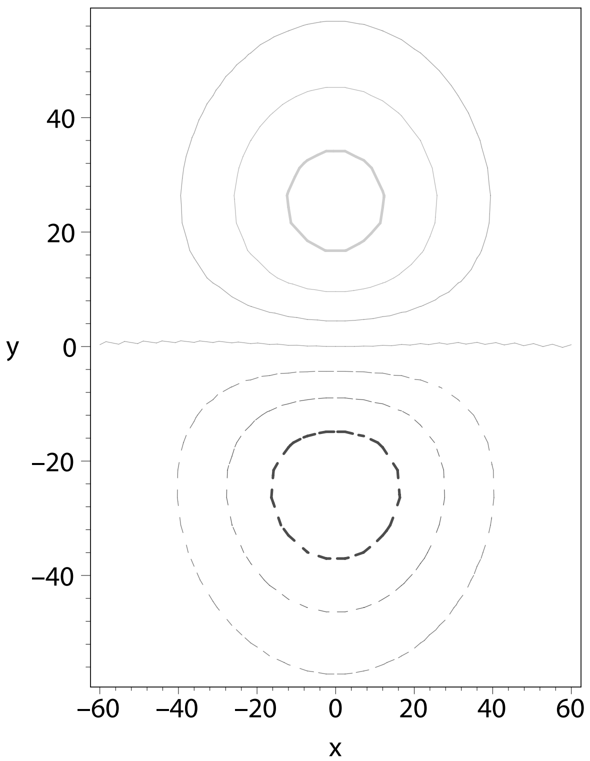

Fig. 3. Wind power input for a Northern Hemisphere Gaussian anticyclone under a uniform westerly wind. Parameters chosen to represent an unresolved midlatitude eddy, see text for details. CI = 1 mW/m^2. Dashed for negative.

three rows of Table 1.

The first four rows of Table 1 imply that the WPI depends mostly upon the time mean winds working on the time mean currents, mostly over length scale larger than 400 km wavelength. How reliable are these larger scale currents? Recall that Scott (1999b) found that, because the wind stress was found to be uncorrelated with the geoid gradient errors, the JGM-03 geoid contributed only about 6.4% error, using the full error covariance matrix out to spherical harmonic degree and order 70. The GGM03C geoid from GRACE has errors at least 50 times smaller than JGM-03 (John Ries, personal communication). Thus we expect the error due to the mean currents to be quite small, and completely dominated by error due to wind stress.

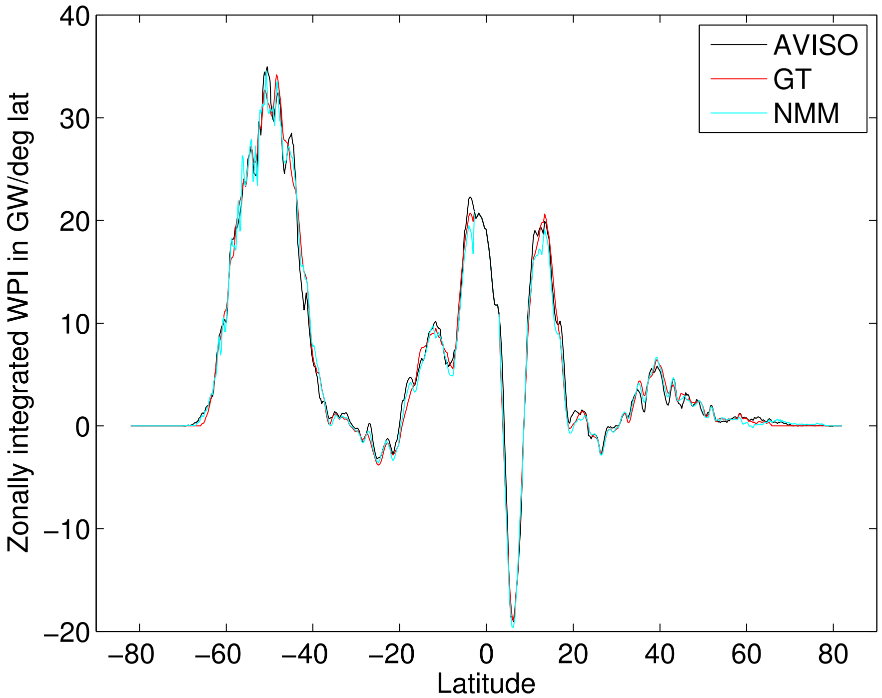

Fig. 4. Zonal integral of $\dot{W}_g$. Data products correspond to the first three rows of Table 1. The black, red and cyan lines correspond to rows one, two and three. Only the time mean currents differ, confirming the insensitivity to these data.

4.2 Uncertainty arising from uncertainty in wind stress

Rows 5 through 8 address the uncertainty due to wind stress (the same current product is used for each). For row 5, only the bulk algorithm relating $\vec{U}_a$ and stress was changed, from the Liu and Tang algorithm to the Large and Pond algorithm. The WPI dropped from $0.91 \rightarrow 0.86$TW, suggesting that this uncertainty is small but not negligible. The 6th row uses the GSSFT2 wind stress, which is completely independent of QuikSCAT wind stress. The WPI is only slightly larger than our best estimate in row 1 (0.95 compared to 0.91TW), providing impressive, independent vindication. Note that much of the increase in row 5 can be associated with the eddy term. The reduction in WPI via the surface current effect on stress may be imperfect because of both the poorer spatial resolution of the GSSFT2 data, and because the wind directions are taken from reanalysis products, which provide absolute, not relative, wind vector directions.

The next two rows, rows 7 and 8 use the best available global reanalysis products. Not adjusting for the surface current effect on stress (numbers in parentheses: 1.09 TW for NCEP2 and 1.28 TW for ERA-40), they overestimate WPI. This overestimate using the reanalysis products is to be expected because of the systematic bias arising from the surface current effect on stress, discussed in section 2.

After roughly accounting for the surface current effect on stress, the reanalysis products give lower WPI values, more in line with our QuikSCAT best estimate (compare WPI not in parentheses). The implication is that all the wind stress products are in remarkable agreement, with discrepancy arising mostly because of the imperfect estimation of the ocean current effect on stress in the reanalysis products. Recall that in roughly accounting for the surface current effect on stress we had to apply a filter to smooth the current fields, see section 3.3. The Gaussian filter of 2° longitude and similar meridional distance was convolved over a square of width 6° longitude. This creates missing data near coasts, which accounts for instance, for the NCEP2 calculation only having good data over 82% of the reference area, see row 7, last column of Table 2. Remarkably, the WPI estimated using smoothed velocities in equation 3 had negligible difference from that obtained with unsmoothed velocities in equation 3. However, the fields looked completely different. The unsmoothed velocities $\dot{W}_g$ map looks strikingly similar to Fig. 1, with spatial correlation $r = 0.979$ (not shown). The smoothed velocities $\dot{W}_g$ map is plotted in Fig. 5.

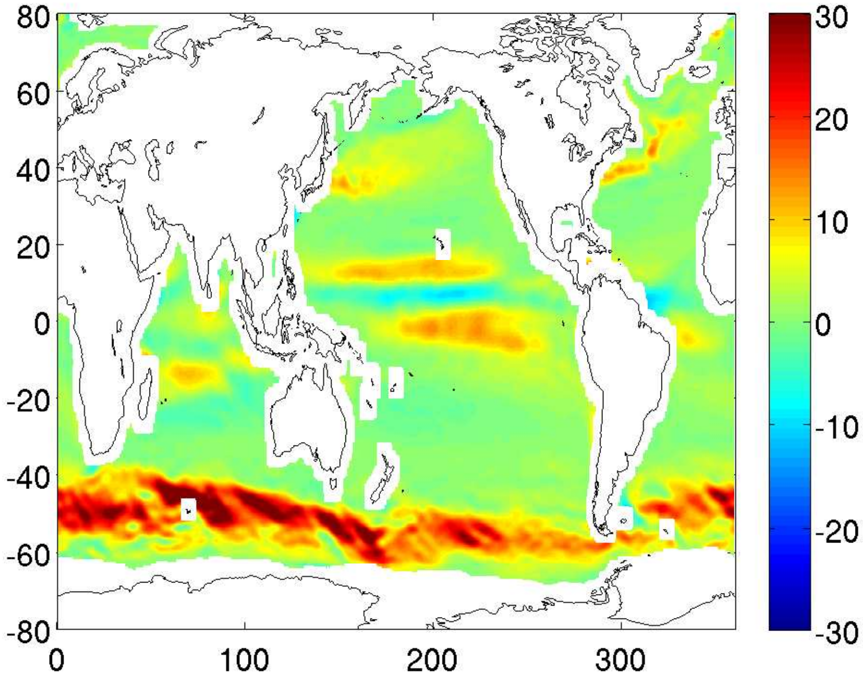

Fig. 5. $\dot{W}_g$ using NCEP2 winds and updated AVISO currents, *i.e.* corresponding to row 7 of Table 1. Missing data near coasts largely results from smoothing. Smoothed currents, see section 3.3, were used to calculate $\dot{W}_g$ in eqn 3. Using unsmoothed currents in eqn 3 gave almost identical WPI, but the $\dot{W}_g$ map strongly resembles Fig. 1.

4.3 Statistical uncertainty and data coverage

The final two rows use the only uniform data available over two 6-year periods. They agree in WPI to within 4%, confirming the statistical significance of the global mean results. Note however, that the eddy-WPI differs by almost a factor of two. Due to the small size of the eddy-WPI, even these small changes of 39 GW represent large fractional changes. Comparing rows 7 and 10 provides another opportunity to see the influence of altimeter data quality, since they use the same stress (NCEP2), but different currents (updated vs. reference altimeter product). WPI agrees within 2% here and eddy-WPI differs only by 3 GW.

The best estimate had data coverage of $3.14 \times 10^{14}\text{m}^2$ or about 86% of the World Ocean. Because most of the missing region is in the Arctic Ocean where the wind stress is weaker than the global average, and where sea ice absorbs much of the wind power input (Hopkins, 1996), we expect missing data is not a serious limitation.

5 Conclusion

Our error estimates are far from rigorous, but the balance of evidence presented above suggests a range of 0.86 to 1.02 TW for the global, time mean, wind power input, WPI. Almost all of this WPI is due to the mean wind stress working on the mean surface geostrophic current. The eddy-WPI found with high-resolution QuikSCAT wind stress is between about 22 to 25 GW. Lower resolution wind products exaggerate the eddy-WPI, to about 40 to 88 GW, after roughly accounting for the surface current effect on stress.

The uncertainty arising from the currents is now dominated by wind stress uncertainty thanks largely to: the GRACE mission, developments to combine surface drifter and *in situ* data to obtain the time mean flow at length scales not resolved by GRACE, and methodologies to effectively combine multiple satellite altimeters. The uncertainty arises almost entirely due to wind stress errors. The uncertainty in the bulk algorithm is not negligible, but the ocean surface current effect on stress is much more important, and can only be approximated in the reanalysis winds. Accurate estimates of the WPI are needed to help quantify the global oceanic mechanical energy budget, as motivated in the Introduction.

A Details of the data and its processing

We discovered that the QuikSCAT Level-3 wind stress product had a missing factor of air density in the Large and Pond algorithm data. We decided it was safer to work with the wind data. We used the QuikSCAT Level-3 winds (PO.DAAC product 109) produced in February and March of 2007. Some problems where identified. In particular, we discovered that there are a few dozen data points for each pass with very extreme values of wind speed for 2003, part of 2004, and 2005. We confirmed with PO.DAAC that this problem arises due to a bug in their processing. To eliminate this bad data, we eliminated all data with wind speeds greater than 50 m/s. As recommended by PO.DAAC, we also eliminate data with the rain flag set to 2 or 6, or with count of zero.

Several different orders of operation are possible in executing Eqn 3. In most cases the different choices made little difference, but some made a surprising difference. Here we detail these dependencies as explored with the QuikSCAT winds and updated AVISO currents (data of row one in Table 1 above). The main result is that, because of the nonlinear dependence of stress upon wind speed, and the high frequency of wind fluctuations, any processing that reduces the wind variability has a noticeable reduction on stress WPI. Other processing details had little influence.

First we report in row 1 of Table A1, the result from row 1 of Table 1 but to more significant digits. Recall this is for daily stress values averaged to weekly values, so that no temporal interpolation of the weekly altimeter data was necessary. All other rows of Table 1 used daily currents.

To minimize the damping of the winds, we decided the best procedure was to convert the ascending and descending pass vector winds immediately to stress values. Then these stresses were averaged to form daily averages. These daily averaged stresses were interpolated to the $1/3°$ longitude Mercator grid of the AVISO currents via bilinear interpolation. The AVISO currents were interpolated to daily values via linear interpolation. The dot product of daily stress with daily currents on the AVISO grid gave the daily WPI, the time average of which give the results shown in row 2 of Table A1. The difference from row 1, that obtained with weekly averages, is less than 1 GW, is much less than that associated with data errors.

One might argue that averaging the ascending and descending pass vector winds gives a better estimate of the daily averaged winds. (However, this is at the expense of damping some of the high-frequency variability inherent in the true wind field.) From these daily winds we computed the daily stress. We then continued as described for the 2nd row (interpolated daily stress to AVISO grid, computed dot product with daily surface currents, etc.). This method produced the lowest results, more than 43 GW lower than the best method, compare rows 2 and 3 of Table A1. Because of the squared dependence of stress upon wind speed, any reduction in the latter has a larger influence on the former, and ultimately on WPI.

For fair comparison with the effect of surface current reduction in stress removed, we had to change the order of the above procedure. We first interpolated the ascending and descending pass vector winds to the AVISO grid, then continued with the processing as described above. This trivial difference actually made a small, almost 7 GW, but noticeable difference in WPI (that would have been attributed to the surface current effect had we not done this test), compare rows 2 and 4 of Table A1. Note that linear interpolation tends to damp the variability, and because of the squared dependence of stress upon wind speed, this damping has an even stronger influence upon WPI. (So in general it would be best to interpolate the stress.)

In row 5 of Table A1 we report the effect of removing the surface current influence on stress in the WPI calculation. This corresponds to the result in parentheses in Table 1.

Acknowledgements

Helpful conversations with Rui Xing Huang and Brian Arbic are gratefully acknowledged. NCEP/DOE AMIP-II Reanalysis data provided by Data Support Section, CISL/NCAR, Boulder, Colorado. ECMWF ERA-40 data used in this study/project have been provided by ECMWF/have been obtained from the ECMWF data server. The Goddard Satellite based Surface Turbulent Fluxes (version-2), GSSTF2, were obtained from the Asia-Pacific-Data-Resource-Center. QuikSCAT and GRACE-Tellus data were obtained from JPL's PO.DAAC website. Specifically, the GRACE-Tellus mean dynamic topography was obtained from http://gracetellus.jpl.nasa.gov/dot.html. The 1992-2002 mean ocean dynamic topography data has been obtained from Nikolai Maximenko (IPRC) and Peter Niiler (SIO). The altimeter products were produced by Ssalto/Duacs and distributed by Aviso, with support from Cnes. RBS and YX were supported by NSF grant OCE-0526412. YX also received support from the UT Jackson School of Geosciences.

References

Alford, M., 2003. Improved global maps and 54-year history of wind-work on ocean inertial motions. Geophys. Res. Lett. 30, art. no. 1424.

Arbic, B. K., MacAyeal, D. R., Mitrovica, J. X., Milne, G. A., 2004. Palaeoclimate: Ocean tides and Heinrich events. Nature 432, doi:10.1038/432460a.

Brunke, M. A., Fairall, C. W., Zeng, X., Eymard, L., Curry, J. A., 2003. Which bulk aerodynamic algorithms are least problematic in computing ocean surface turbulent fluxes? J. Climate 16, 619–635.

Bye, J. A. T., 1985. Large-scale momentum exchange in the coupled atmosphere ocean. In: Nihoul, J. (Ed.), Coupled ocean-atmosphere models. Elsevier oceanography series ; 40. Elsevier, Ch. 6, pp. 51–61.

Chelton, D. B., Freilich, M. H., 2005. Scatterometer-based assessment of 10-m wind analyses from the operational ECMWF and NCEP numerical weather prediction models 133, 409–429.

Chou, S.-H., Nelkin, E., Ardizzone, J., Atlas, R. M., Shie, C.-L., 2004. Surface turbulent heat and momentum fluxes over global oceans based on the goddard satellite retrievals, version 2 (GSSTF2). J. Climate 17, 3256–3273.

Dawe, J. T., Thompson, L., 2006. Effect of ocean surface currents on wind stress, heat flux, and wind power input to the ocean. Geophys. Res. Lett., Art. No. L09604.

Ducet, N., LeTraon, P.-Y., Reverdin, G., 2000. Global high-resolution mapping of ocean circulation from TOPEX/Poseidon and ERS-1 and -2. J. Geophys.

Res. 105 (C8), 19477–19498.

Duhaut, T. H., Straub, D. N., 2006. Wind stress dependence on ocean surface velocity: Implications for mechanical energy input to ocean circulation. J. Phys. Oceanogr. 36, 202–211.

Hopkins, M. A., 1996. On the mesoscale interaction of lead ice and floes. J. Geophys. Res. 101, 18315–18326.

Huang, R. X., Wang, W., Liu, L. L., 2006. Decadal variability of wind-energy input to the world ocean. Deep-Sea Res. II 19, 31–41.

Hughes, C. W., Wilson, C., 2008. Wind work on the geostrophic circulation: an observational study of the effect of small scales in the wind stress. J. Geophys. Res. 113, C02016.

Kanamitsu, M., Ebisuzaki, W., Woolen, J., Potter, J., Fiorion, M., 2000. An overview of NCEP/DOE reanalysis-2. In: Proc. 2nd Int. Conf. on Reanalyses. WMO, Reading, U.K., pp. 1–4.

Kelly, K. A., 2004. Wind data: A promise in peril. Science 303, 962–963.

Kistler, R. E., Kalnay, E. M., Collins, W., Saha, S., White, G., Woollen, J., Chelliah, M., Ebisuzaki, W., Canamitsu, M., Kousky, V., van den Dool, H., Jenne, R., Fiorinio, M., 2001. The NCEP/NCAR 50-year reanalysis: Monthly means CD-ROM and documentation. Bull. Amer. Met. Soc. 82, 247–267.

LeTraon, P.-Y., Dibarboure, G., Ducet, N., 2001. Use of a high-resolution model to analyze the mapping capabilities of the multi-altimeter missions. J. Atmos. Oceanic Technol. 18, 1277–1288.

LeTraon, P.-Y., Nadal, F., Ducet, N., 1998. An improved mapping method of multisatellite altimeter data. J. Atmos. Oceanic Technol. 15, 522–534.

Munk, W., Wunsch, C., 1998. Abyssal recipes II. Energetics of tidal and wind mixing. Deep-Sea Res. 45, 1977–2010.

Niiler, P. P., Maximenko, N. A., McWilliams, J. C., 2003. Dynamically balanced absolute sea level of the global ocean derived from near-surface velocity observations. Geophys. Res. Lett. 30 (22), 2164.

Oort, A. H., Anderson, L. A., Peixoto, J. P., 1994. Estimates of the energy cycle of the oceans. J. Geophys. Res. 99 (C4), 7665–7688.

Pascual, A., Pujol, M.-I., Larnicol, G., LeTraon, P.-Y., Rio, M. H., Hernandez, F., 2007. Mesoscale mapping capabilities of multisatellite altimeter missions: First results with real data in the Mediterranean Sea. J. Mar. Sys. 65, 190–211.

Perry, K. L., 2001. Seawinds on QuikSCAT level 3 daily, gridded ocean wind vectors (JPL SeaWinds project). Online document, available at [http://poseidon.jpl.nasa.gov:2031/DATASET_DOCS/qscat_L3.html].

Plueddemann, A., Farrar, J. T., 2006. Observations and models of the energy flux from the wind to mixed-layer inertial currents. Deep-Sea Res. II 53, 5–30.

Ralph, E. A., Niiler, P. P., 1999. Wind driven currents in the tropical Pacific. J. Phys. Oceanogr. 29, 2121–2129.

Reigber, C., Schmidt, R., Flechtner, F., Knig, R., Meyer, U., Neumayer, K.-H., Schwintzer, P., Zhu, S. Y., 2005. An earth gravity field model complete to degree and order 150 from GRACE: EIGEN-GRACE02S. Journal of Geodynamics 39 (1), 1–10.

Rio, M.-H., Hernandez, F., 2004. A mean dynamic topography computed over the world ocean from altimetry, in-situ measurements and a geoid model. J. Geophys. Res. 109 (C12), Art. No. C12032.

Scott, R. B., 1999a. Geostrophic energetics and the small viscosity behaviour of an idealized ocean circulation model. Ph.d.

dissertation, McGill University, Montreal, PQ, [Available from http://www.ig.utexas.edu/people/staff/rscott/].

Scott, R. B., 1999b. Mechanical energy flux to the surface geostrophic flow using TOPEX/poseidon data. In: 23^{rd} EGS General Assembly. Vol. 24 of Physics and Chemistry of the Earth Part A – Solid Earth and Geodesy. European Geophysical Soceity, Nice, France, pp. 399–402.

Scott, R. B., Wang, F., 2005. Direct evidence of an oceanic inverse kinetic energy cascade from satellite altimetry. J. Phys. Oceanogr. 35, 1650–1666.

Stammer, D., 1997. Global characteristics of ocean variability estimated from regional TOPEX/Poseidon altimeter measurements. J. Phys. Oceanogr. 27, 1743–1769.

Tapley, B. D., Chambers, D. P., Bettadpur, S., Ries, J. C., 2003. Large scale ocean circulation from the grace GGM01 geoid. Geophys. Res. Lett. 30 (22), Art. No. 2163.

von Storch, J.-S., Sasaki, H., Marotzke, J., 2007. Wind-generated power input to the deep ocean: an estimate using a $1/10°$ general circulation model. J. Phys. Oceanogr. 37 (3), 657–672.

Wang, W., Huang, R. X., 2004a. Wind energy input to the Ekman layer. J. Phys. Oceanogr. 34, 1267–1275.

Wang, W., Huang, R. X., 2004b. Wind energy input to the surface waves. J. Phys. Oceanogr. 34, 1276–1280.

Watanabe, M., Hibiya, T., 2002. Global estimates of the wind-induced energy flux to inertial motions in the surface mixed layer. Geophys. Res. Lett. 29, 10.1029/2001GL014422.

Wittenberg, A., 2004. Extended wind stress analyses for ENSO. J. Climate 17, 2526–2540.

Wunsch, C., 1998. The work done by the wind on the oceanic general circulation. J. Phys. Oceanogr. 28, 2332–2340.

Wunsch, C., Ferrari, R., 2004. Vertical mixing, energy, and the general circulation of the oceans. Ann. Rev. Fluid Mech. 36, 281–314.

Xu, Y., Scott, R. B., 2008. Subtleties in forcing eddy resolving ocean models with satellite wind data. Ocean Modelling 20, 240–251.

Table 1. Time: a = 1/2/1994 - 12/31/1999, b = 1/2/2000 - 12/31/2005; Wind stress: QS = QuikSCAT, TL = Tang and Liu, LP = Large and Pond; Currents: upd = updated, ref = reference, GT mean = GRACE-Tellus mean dynamic topography poleward of 3°, NMM mean = Maximenko mean dynamic topography poleward of 3°; Eddy is the eddy-WPI in TW; Total is total WPI in TW; Area is the percentage of the reference area with data. The reference area was $3.14 \times 10^{14} \mathrm{m}^2$, as shown in Fig. 1. Numbers in parentheses do not take into account the bias arising from the surface current effect on stress described above.

			global			extraequatorial		
Time	$\vec{\tau}$	$\vec{u}_g$	eddy	total	area	eddy	total	area
b	QS TL	Aviso upd	0.024 (0.23)	0.91 (1.2)	100	0.001	0.81	100
b	QS TL	GT mean	0.024	0.90	93.5	0.002	0.80	98
b	QS TL	NMM mean	0.024	0.90	97.7	0.002	0.78	98
b	QS TL	Aviso ref	0.025	0.91	100	0.003	0.81	100
b	QS LP	Aviso upd	0.022	0.86	100	0.001	0.76	100
a	GSSFT2	Aviso upd	0.088	0.95	86.6	0.047	0.84	86
b	NCEP2	Aviso upd	0.076 (0.12)	1.0 (1.1)	82.0 (100)	0.062 (0.092)	0.094 (1.0)	82 (100)
a	ERA-40	Aviso upd	0.087 (0.17)	0.99 (1.3)	81.9 (100)	0.057 (0.13)	0.90 (1.17)	82 (100)
a	NCEP2	Aviso ref	0.040	0.98	81.9	0.031 (0.051)	0.91 (0.96)	82 (100)
b	NCEP2	Aviso ref	0.079	1.02	82.0	(0.089)	(1.0)	(100)

Table 1 Sensitivity to data processing and order of operations. All calculations use the same data over the same time period (corresponding to row 1 of Table 1: Time: 1/2/2000 - 12/31/2005; Wind stress: QuikSCAT, TL = Tang and Liu; Currents: upd = updated AVISO; The area of good data was $3.14 \times 10^{14}\mathrm{m}^2$). Numbers show more digits than are significant given the data limitations. Asc and des refer to the ascending and descending passes of the QuikSCAT satellite, ave. = linear average; "regrid" means bilinear interpolation from 1/4° latitude and longitude QuikSCAT grid to 1/3° longitude Mercator AVISO grid. All rows use AVISO currents interpolated to daily values, except for row one, which used weekly AVISO currents.

Order of operations	$\dot{W}_g$ [TW]
Asc. des. passes → stress → daily ave.→ weekly ave.→ regrid	0.90769
Asc. des. passes → stress → daily ave.→ regrid	0.90824
Asc. des. passes → daily ave. → stress → regrid	0.86481
Asc. des. passes → regrid → stress → daily ave.	0.90149
Asc. des. passes → regrid → add $\vec{u}_g$ → stress → daily ave.	1.1943